Tsunami hazard mapping and wave propagation analysis through numerical model simulations scenario: Case study Labuan Bajo, East Nusa Tenggara

Muhammad A. Ma'rup[1], *Franto* Novico[2,3], and *Agus S.* Atmadipoera[1*]

[1]Marine Sciences and Technology Program, Faculty of Fisheries and Marine Sciences, IPB University, Bogor, Indonesia
[2]Research Center for Geological Disaster, National Research and Innovation Agency (BRIN), Bandung, Indonesia
[3]Marine Geological Institute (MGI), Ministry of Energy and Mineral Resources, Bandung, Indonesia

Abstract. Indonesia's topographical and tectonic configuration makes many coastal areas, including Labuan Bajo in East Nusa Tenggara, highly susceptible to tsunami threats. As a growing tourism center, Labuan Bajo necessitates comprehensive tsunami risk assessments to support disaster mitigation and coastal planning. This paper presents tsunami hazard mapping and wave propagation analysis through numerical simulations across six earthquake scenarios. The MIKE 21 Flow Model FM was utilized to predict tsunami wave dynamics, integrating high-resolution bathymetric data, earthquake mechanisms, and tidal fluctuations. Scenarios were based on potential rupture zones along the Flores Sea subduction area, illustrating both worst-case and moderate events. The models yielded estimates of wave height, arrival time, and tsunami energy at six coastal and nearshore observation stations. Results show considerable variation in wave heights, with peaks over 7 meters in severe cases. Arrival times ranged from 6 minutes to nearly 2 hours, indicating both near-field and far-field threats. Hazard maps highlight areas with high exposure, especially low-lying and densely populated zones. These findings underscore the necessity of incorporating numerical modeling into early warning systems, evacuation planning, and coastal infrastructure design. This study enhances understanding of tsunami hazards and provides recommendations to strengthen resilience in vulnerable, tourism-dependent coastal communities like Labuan Bajo.

Keywords: Tsunami, Labuan Bajo, MIKE 21, numerical modelling

* Corresponding author: atmadipoera_itk@apps.ipb.ac.id

1 Introduction

Indonesia is highly vulnerable to earthquakes and tsunamis due to its location between the Indo-Australian and Pacific tectonic plates [1, 2]. Subduction zones, often called megathrusts, extend from west Sumatra to the south of Java, Bali, Nusa Tenggara, and northern Papua, marking active plate boundaries [3]. Tsunami sources include seismic and nonseismic events, and nearly all Indonesian coasts face such risks [3]. East Nusa Tenggara, particularly Flores, is one of the most tsunami-prone areas, with ten recorded events, six from earthquakes and other landslides or volcanic eruptions [4].

Tectonic activity in the Timor Trough and Flores Thrust continues to intensify, as indicated by increased interactions between tectonic plates, which is likely to trigger more earthquakes and ground deformation in the future [5, 6]. Most of the deformation resulting from plate convergence is concentrated in the Timor Trough and the Flores Back-arc Thrust zone [6], as shown in **Fig. 1**. Labuan Bajo, the capital of West Manggarai, hosts 226,560 residents and 186 islands, making it both a tourism hub and disaster-prone area [7]. Spatial planning should integrate disaster mitigation as a national tourism priority. In 2023, East Nusa Tenggara Province received 824,428 visitors, including 80,000 international tourists [7]. Behind the beauty of the islands, Flores, including Labuan Bajo, have experienced potential earthquakes of Mw 7.5–8.5 [8]. Therefore, tsunami modeling and simulations are essential for raising awareness and supporting mitigation strategies [9]. This study aims to determine the tsunami wave height and arrival time in the waters of Labuan Bajo using tsunami wave modeling based on the worst-case earthquake scenario in the Flores Sea subduction zone.

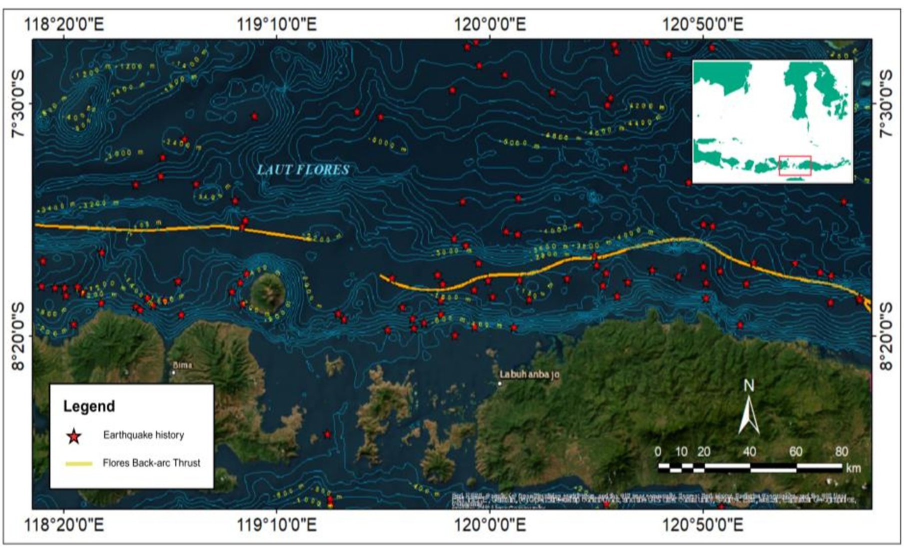

Fig. 1. Earthquake history (>5 Mw) in the Flores Backarc Thrust region from 1800 to 2025 (modified from USGS).

2 Methodology

2.1 Data

This study utilizes bathymetric data from Batimetri Nasional (BATNAS) with a spatial resolution of 6 arc-second [10], shoreline shapefiles of Flores Island and the surrounding islands in Labuan Bajo from the tanahair.indonesia, earthquake parameters along with source mechanisms obtained from USGS, Global CMT, Indonesian Agency for Meteorology, Climatology, and Geophysics (BMKG), the Ministry of Energy and Mineral Resources (KESDM), and tidal data from the Mike Tidal Toolbox: Tide Prediction of Heights.

2.2 Earthquake sources

The earthquake sources for the tsunami modeling were located in the Flores Sea, north of Flores Island, with six epicenters selected based on the earthquake history compiled from the USGS (**Fig. 2**). Once the sources were defined, observation points (**Fig. 2**) were strategically placed along the coast and surrounding areas to represent the key locations at risk. The numerical outputs from these points were extracted from the model simulations in the form of a sea surface elevation time series.

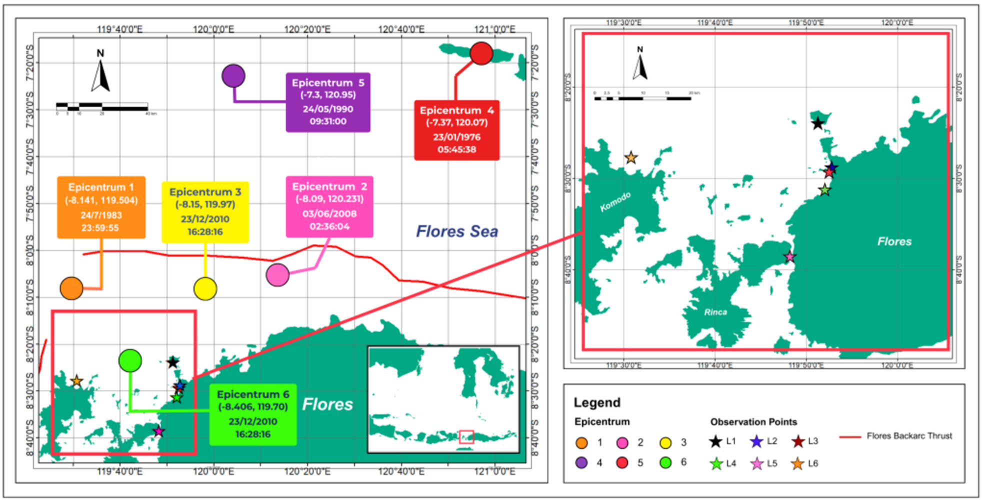

Fig. 2. Six Earthquake sources based on earthquake history in Flores Sea for tsunami modeling and the observation points.

2.3 Generating initial conditions

The initial condition of the simulation was the tsunami wave height generated at the earthquake source, calculated using the MIKE 21 Seismology Toolbox. Bathymetry data served as an input. The MIKE 21 Seismology toolbox applies Okada's (1985) method to model seabed deformation based on rectangular fault dimensions. Fault dimensions are defined by four key parameters: length (L), which describes the horizontal extent of the fault plane; width (W), indicating its down-dip extent; fault area (S); slip (u); and the average vertical displacement across the fault surface [11]. This study adopts a subduction dip-slip fault mechanism, and the scaling laws of [12] were applied to estimate L, S, W, and u. The earthquake parameters for the simulation were obtained from the USGS and Global CMT records of the Flores Backarc Thrust. These were upscaled to develop the worst-case tsunami scenarios. The output provides the initial tsunami surface elevation in dfs2 format. The compiled parameters of the six sources are listed in **Table 1**.

Table 1. The input parameters for the initial condition were generated using the MIKE 21 Seismology Toolbox.

Parameter	Earthquake Sources (Scenarios)					
	1	**2**	**3**	**4**	**5**	**6**
Dip (°)	67	67	78	38	25	84
Slip (°)	75	85	81	96	107	154
Strike (°)	253	259	242	233	46	308
Depth (km)	30	18	38	35	45	12
Latitude (°)	-8.141	-8.09	-8.15	-7.37	-7.3	-8.40
Longitude (°)	119.504	120.231	119.97	120.07	120.95	119.70
Fault Mechanism	Subduction Dip-Slip	Subduction Dip-Slip	Subduction Dip-Slip	Subduction Dip-Slip	Subduction Dip-Slip	Subduction Dip-Slip
Mw	8.5	8.5	8.5	8.5	8.5	8.5
Shear (GPa)	39.7	39.7	69.8	69.8	69.8	39.7
Lambda (GPa)	32.1	32.1	66.4	66.4	66.4	32.1
Initial Rupture Time	24/7/1983 23:59:55	03/06/2008 02:36:04	23/12/2010 16:28:16	23/01/1976 05:45:38	24/05/1990 09:31:00	20/01/2012 20:32:55

2.4 Numerical modeling

Tsunami propagation is simulated using a cell-based Finite Volume Method (FVM) on an unstructured mesh with explicit time stepping, applicable in Cartesian or spherical coordinates [13]. The MIKE 21 Flow Model uses a nested grid system, which is essential for simulating tsunamis in coastal areas with complex geometries [11]. The governing partial differential equations are the continuity and momentum equations presented in Equation (1), with momentum transfer along the x -axis in Equation (2) and the y -axis in Equation (3).

$$\frac{\partial h}{\partial t}+\frac{\partial h\bar{u}}{\partial x}+\frac{\partial h\bar{v}}{\partial y}=hS \tag{1}$$

$$\frac{\partial h\bar{u}}{\partial t}+\frac{\partial h\overline{u^2}}{\partial x}+\frac{\partial h\bar{v}}{\partial y}=f\bar{v}h-gh\frac{\partial \eta}{\partial x}-\frac{h}{\rho_0}\frac{\partial p_a}{\partial x}+\frac{gh^2}{2\rho_0}\frac{\partial \rho}{\partial x}+\frac{\tau_{sx}}{\rho_0}-\frac{\tau_{bx}}{\rho_0}-\frac{1}{\rho_0}\left(\frac{\partial S_{xx}}{\partial x}+\frac{\partial S_{xy}}{\partial y}\right)+\frac{\partial}{\partial x}(hT_{xx})+\frac{\partial}{\partial y}(hT_{xy})+h\overline{u_s}S \tag{2}$$

$$\frac{\partial h\bar{v}}{\partial t}+\frac{\partial h\overline{uv}}{\partial x}+\frac{\partial h\overline{v^2}}{\partial y}=-f\bar{u}h-gh\frac{\partial \eta}{\partial y}-\frac{h}{\rho_0}\frac{\partial p_a}{\partial y}+\frac{gh^2}{2\rho_0}\frac{\partial \rho}{\partial y}+\frac{\tau_{sy}}{\rho_0}-\frac{\tau_{by}}{\rho_0}-\frac{1}{\rho_0}\left(\frac{\partial S_{yx}}{\partial x}+\frac{\partial S_{yy}}{\partial y}\right)+\frac{\partial}{\partial x}(hT_{xy})+\frac{\partial}{\partial y}(hT_{yy})+h\overline{v_s}S \tag{3}$$

Where $h=\eta+d$ is the total water depth; η is the free surface elevation; d is the still water depth; x, y are Cartesian coordinates; u, v are velocity components in the x and y directions; $\bar{u}, \bar{v}$ are depth-averaged velocities; g is gravitational acceleration; f is the Coriolis coefficient; $f\bar{u}$, $f\bar{v}$ are accelerations due to Earth's rotation; p_a is atmospheric pressure; ρ_0 is mean seawater density; ρ is local seawater density; S_{xx}, S_{xy}, S_{yx}, S_{yy} are radiation stress components; T_{xx}, T_{xy}, T_{yy} are horizontal viscous stress components; S is the source/sink term; u_s, v_s are inflow and outflow velocities.

2.5 Model scenarios

2.5.1 Boundaries condition

In this study, the open boundaries were divided into five sections: West, North, East A, East B, and South (**Fig. 3**. Tidal forcing was applied at each boundary using varying time- and along-boundary formats. The tidal data were generated using the MIKE 21 Tidal Toolbox (Tide Prediction of Heights) by inputting coordinate points for each boundary, adjusted to match the timing of the earthquake and tsunami events. Output data in .The dfs1 (time series) format serves as a boundary condition input for the MIKE 21 Flow Model FM.

Tidal data were incorporated to represent the actual ocean conditions during the tsunami. Although earlier studies often disregarded tidal effects in tsunami mitigation [14], recent research has highlighted their significant influence on tsunami dynamics. In shallow waters, the interaction between tides and tsunami waves can significantly affect wave height [15]. These findings strongly suggest that tidal effects should be considered in tsunami analysis.

2.5.2 Input parameters for the hydrodynamic module

The main input parameters for the tsunami modelling in the MIKE 21 Flow Model are summarized in **Table 2**. A time step of 5 s was applied to simulate three hours of tsunami propagation, ensuring sufficient temporal resolution and capturing the full wave dissipation. Because the model uses an explicit scheme, the time step must satisfy the Courant–Friedrichs–Lewy (CFL) condition (<1) to maintain stability. In deep and open ocean settings, continuity across domains with different spatial grids can be achieved by adjusting Δx while maintaining Δt constant [16].

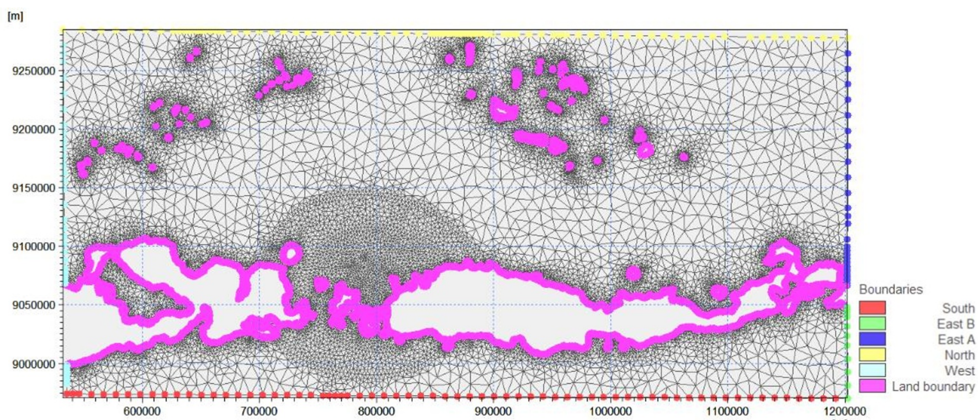

Fig. 3. Boundaries condition of Nusa Tenggara and small islands in Flores Waters for Hydrodynamic module.

The numerical scheme was set to a higher order to improve the model accuracy, whereas the bed resistance was parameterized using the Manning number. According to the MIKE 21 Hydrodynamic Module User Guide, significant variations in water depth require the specification of Manning's roughness coefficient, with typical values ranging from 20 to 40 $m^{1/3}/s$; in the absence of more accurate field data, a value of 32 $m^{1/3}/s$ is commonly applied. The initial water conditions at the time of the earthquake were incorporated into the Hydrodynamic Module, after which the model was executed for the two earthquake sources.

https://doi.org/10.1051/bioconf/202622006003

Table 2. The input parameters for the hydrodynamic module.

Parameter	**Value**
No. of Time Steps	2880
Parameter	**Value**
Time Step	5 s
Critical Courant-Friedrichs-Lévy (CFL) Number	0.8
Run Duration	6-7 hours
Numerical Scheme	Higher Order
Coriolis Force	Varying in Domain
Bed Resistance	32 $m^{1/3}/s$
Initial Condition	Initial Condition Result (.dfs2)
Boundary Condition	-West: Tide (.dfs1) -North: Tide (.dfs1) -South: Tide (.dfs1) -East A: Tide (.dfs1) -East B: Tide (.dfs1)
Output items	Surface elevation, Current Speed, Current Direction

3 Result and discussion

3.1 Initial condition

The water surface deformation resulting from the six earthquake scenarios generated using the MIKE 21 Seismology Toolbox is presented in **Fig. 4**. Source 1 with a maximum height of 1.69 m, source 2 with a maximum height of 2.05 m, source 3 with a maximum height of 1.34 m, source 4 with a maximum height of 1.90 m, source 5 with a maximum height of 1.60 m, and source 6 with a maximum height of 0.85 m. This deformation served as the initial condition, representing sea surface elevation changes induced by tectonic seafloor displacement. The output is stored in . dfs2 format, a two-dimensional grid structure within MIKE 21 designed to represent spatial data in the horizontal domain.

The initial tsunami source orientation and geometry in numerical modeling depend strongly on earthquake fault parameters, such as strike, dip, rake, and slip, as these control the spatial pattern of coseismic seafloor displacement. Variations in these parameters lead to different deformation shapes and directivity patterns of the modeled tsunami source [17].

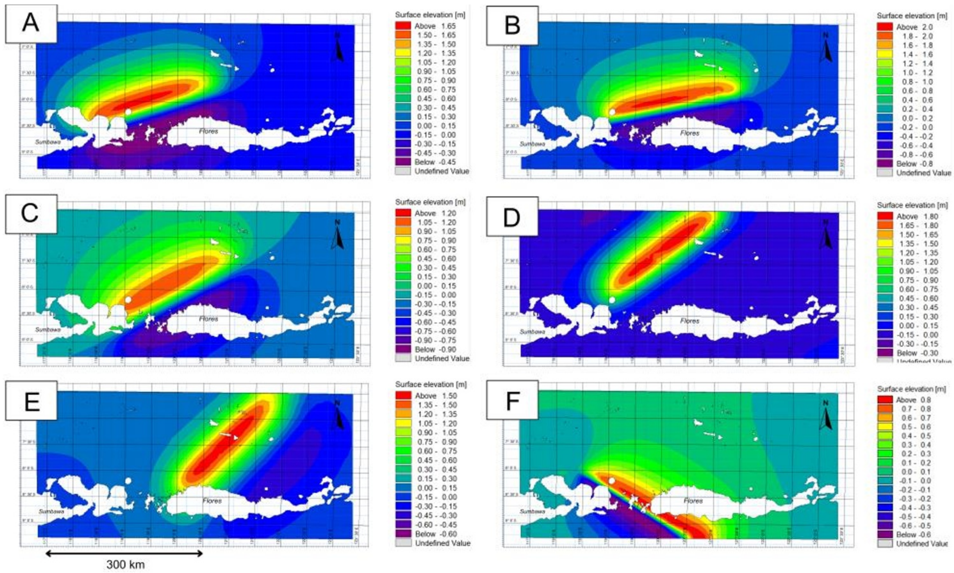

Fig. 4. The initial tsunami conditions in Flores Waters are illustrated as follows: (A) Source 1; (B) Source 2; (C) Source 3; (D) Source 4; (E) Source 5; (F) Source 6

3.2 Tsunami propagation model results

Based on the modelling results (**Fig. 5** and **Fig. 6**), the variations in tsunami height, arrival time, and period across the five earthquake sources are governed by the distance from the epicenter, orientation of each observation point relative to the direction of wave propagation, and seafloor topography. Source 1 generated a maximum wave height of 6.6 m at observation point L5, which was located 76 km away, with an arrival time of 35 min. A similar pattern was found in Source 2, where the largest wave was again recorded at observation point L5, reaching 6.7 m at 146 km with a 38-minute arrival time. In contrast, Source 3 produced its highest wave at observation point L2 with a peak of 7.15 m at a distance of 50 km, arriving approximately 50 min after the earthquake. Source 4 also exhibited a maximum at observation point L5, with a height of 5.68 m at 146 km and an arrival time of 40 min. Source 5 differed by producing its highest wave at observation point L4, where the second wave peaked at 5.23 m at a distance of 179 km, following the initial arrival. Finally, Source 6, the epicenter closest to the observation points, shows a maximum height of 3.18 m at observation point L2, located 25 km from the epicenter.

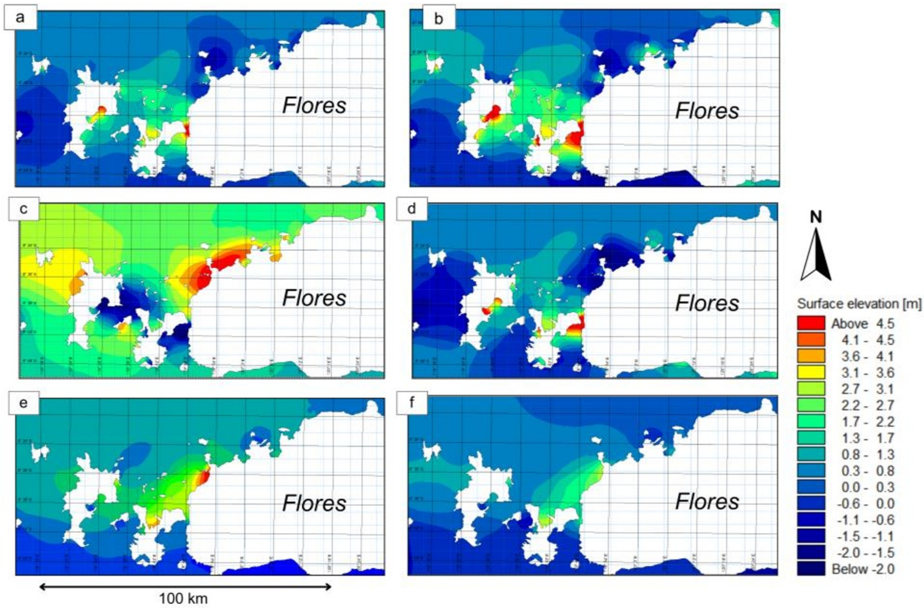

Fig. 5. Visualization of maximum height for each scenario from tsunami propagation results: (a) earthquake source 1; (b) earthquake source 2; (c) earthquake source 3; (d) earthquake source 4; (e) earthquake source 5; (f) earthquake source 6.

The tsunami wave heights were extracted at six predefined observation points to examine the temporal variation in the wave elevation throughout the propagation process. This approach allows for a detailed assessment of how a tsunami evolves as it travels across different locations, reflecting both spatial and temporal dynamics. The time series of the tsunami heights at each observation point is presented in **Fig. 6** (A-F).

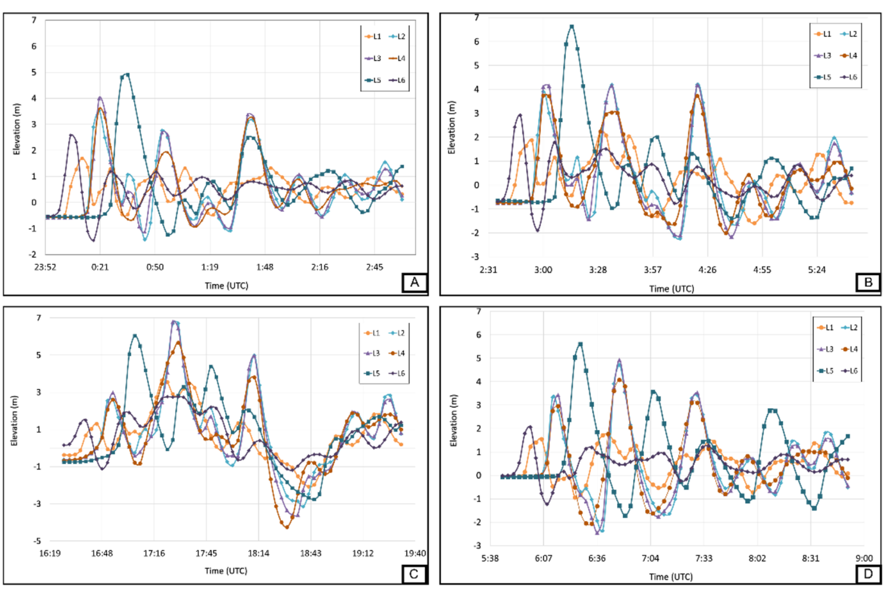

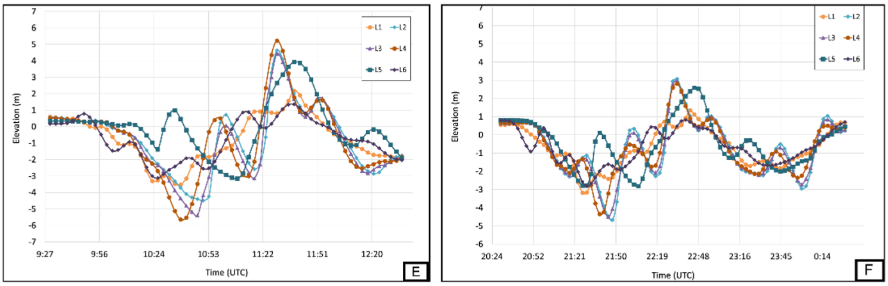

Fig. 6. Time series of tsunami heights at observation points: (A) earthquake source 1; (B) earthquake source 2; (C) earthquake source 3; (D) earthquake source 4; (E) earthquake source 5; (F) earthquake source 6.

3.3 Impact of source location on tsunami wave heights

The maximum tsunami wave height at the shoreline is influenced by multiple factors, namely, the distance between the source and the target area, the azimuthal orientation of the source relative to the coastline, wave scattering caused by local or regional bathymetric features, and amplification along the propagation path resulting from bathymetric processes such as reflection, refraction, and scattering [18]. Therefore, estimating the tsunami wave height and its associated impacts is often uncertain. Small shifts in source location can cause substantial differences in the amplitude and timing of peak waves, whereas adjacent coastlines may experience highly variable wave heights from a single source [16, 17]. However, based on [20], the distribution of tsunami heights is influenced not only by local seabed topography but also by the orientation and shape of the initial condition, which in some cases plays a dominant role in determining the wave height at the shoreline.

To assess the influence of the earthquake source location on tsunami heights along the coast, the sources in this study were classified into three zones: A, B, and C (**Fig. 7**). Zone A represents sources located closest to the shoreline and the observation points, Zone B corresponds to sources situated within the Flores thrust zone, and Zone C encompasses sources positioned farthest from both the Labuan Bajo coastline and thrust zone.

Zone A, which consists of earthquake source 6, is the area closest to the Labuan Bajo coastline, with an average distance of approximately 25 km from the earthquake source to each observation point. This earthquake source region was located in an area with a bathymetric depth of approximately 200 m. The fluctuations in the water surface elevation for this source are shown in **Fig. 6F**. The results indicated an initial drawback lasting for approximately one hour after the earthquake, followed by the arrival of a tsunami approximately one hour later, with maximum wave heights exceeding 3 m at observation points L2, L3, and L4.

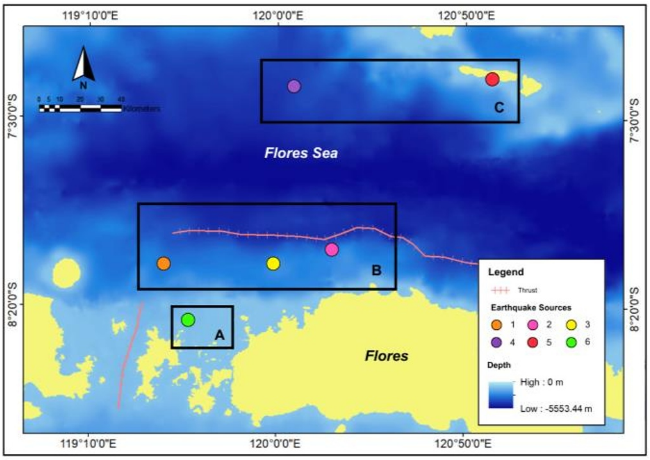

Fig. 7. Earthquake source zones are differentiated in accordance with the characteristics of their respective source regions.

Zone B, located directly within the Flores Sea subduction zone, consists of three earthquake sources (Sources 1, 2, and 3) and is situated at a bathymetric depth of approximately 2000 m. The tsunami wave height fluctuations in this zone are illustrated in **Fig. 6A**, **6B**, and **6C**. The results showed maximum wave heights exceeding 5 m, with Sources 2 and 3 producing the most significant amplitudes. Source 2 generated a wave height of approximately 7 m at observation point L5, whereas Source 3 produced similar heights of approximately 7 m at observation points L3 and L2. The peak tsunami height in this zone reached approximately one hour after the earthquake.

Zone C, which is situated farthest from both the Labuan Bajo coastline and the Flores subduction zone, comprises two earthquake sources (Sources 4 and 5). The tsunami wave fluctuations in this zone are shown in **Fig. 6D** and **Fig. 6E**. Source 4 generated the highest tsunami in this zone, with a maximum wave height of approximately 5 m recorded at observation point L5 approximately 40 min after the earthquake. In contrast, Source 5 produced a prolonged drawback that lasted nearly two hours before the tsunami waves arrived. The maximum wave height for this source reached approximately 3 m, as observed at observation points L2, L3, and L4.

3.4 Discussion

The results from Zones A, B, and C indicate that tsunami characteristics in Labuan Bajo are not determined solely by source proximity or the initial wave height at the source but rather by the combined influence of source orientation, tectonic setting, and local bathymetric conditions [21]. In Zone A, although the sources were located closest to the coastline, the resulting tsunami heights were comparatively modest, generally below 3 m, at several observation points. In contrast, Zone B, situated within the Flores subduction zone and at greater bathymetric depths, generated the largest amplitudes, with wave heights reaching up to 7 m. Zone C, the most distant from both the shoreline and subduction interface, produced smaller wave heights but was characterized by a prolonged drawback phase lasting up to two hours.

These outcomes demonstrate that tsunami impact cannot be explained by a simple correlation with the distance to the source, as stated in previous studies [19]. The relatively low amplitudes generated by the near-field source in Zone A emphasize that bathymetric conditions and source orientation play a decisive role in modulating the tsunami energy before it reaches the coast. Although subduction-related sources (Zone B) pose the greatest hazard potential because of their capacity to generate extreme waves, both near-field (Zone A) and far-field (Zone C) events remain significant because of their unique characteristics: short arrival times in Zone A and prolonged drawbacks in Zone C. These insights underscore the importance of scenario-based hazard assessments, and the need for evacuation strategies tailored to a diverse range of possible tsunami impacts.

The results from all the earthquake scenarios were compiled and further processed into infographic maps illustrating the maximum tsunami heights at each observation point (**Fig. 8**). This visualization provides an overview of the spatial variability of tsunami impacts across different scenarios, highlighting how each site responds differently in terms of intensity and maximum wave height.

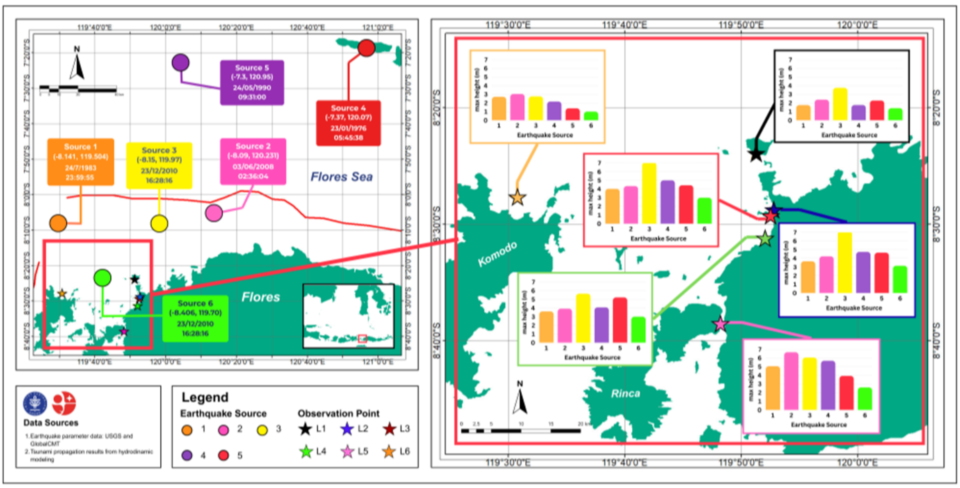

Fig. 8. Infographic map of maximum tsunami heights at observation points in labuan bajo waters based on the worst-case scenario (Mw 8.5 Earthquake).

4 Conclusion

The heights of the tsunami waves were not consistently proportional to their distance from the earthquake epicenter. For instance, despite observation point L1 being in proximity to the epicenter, its amplitude was recorded to be lower than that at more distant locations. This suggests that wave height is affected not only by distance but also by factors such as propagation direction, local bathymetry, and the arrangement of adjacent small islands. Sites situated along the primary propagation axis typically absorb more energy, but a gradual seabed gradient facilitates shoal development and refraction, thereby enhancing wave heights at the shoreline. Consequently, areas such as L5 and L2 consistently exhibited the largest amplitudes, whereas proximal sites showed diminished waves. Because of the intrinsic heterogeneity of tsunami behavior, it is vital to emphasize the significance of scenario-based hazard assessments and the formulation of evacuation procedures customized to the spectrum of potential tsunami impacts.

References

1. C.E. Pangge, K. Subagiada, D. Djayus, Analisis kecepatan tanah maksimum di daerah akibat gempa bumi lombok di daerah pengamatan Labuan Bajo, Waingapu dan

Maumere Nusa Tenggara Timur 05 Agustus Tahun 2018. Geosains Kutai Basin. **5**, 1–6 (2022). https://doi.org/10.30872/geofisunmul.v5i1.730
2. R.I. Ariska Rudyanto, Pemodelan tsunami sebagai bahan mitigasi bencana studi kasus Sumenep dan kepulauannya. J. Neutrino. **2**, 164–182 (2012). https://doi.org/10.18860/neu.v0i0.1639
3. Kementrian Energi dan Sumberdaya Mineral, Katalog tsunami indonesia tahun 416 - 2023 pert Tahun (Badan Meteorologi Klimatologi dan Geofisika, Jakarta Pusat, 2023)
4. M. Wibowo, Modeling the potential of tsunami hazard in Labuan Bajo towards a disaster-resilient tourism area, Indones. J. Geogr. **54**, 83–91 (2022) https://doi.org/10.22146/ijg.71220
5. H. Nugroho, R. Harris, A.W. Lestariya, B. Maruf, Plate boundary reorganization in the active Banda Arc-continent collision: Insights from new GPS measurements. Tectonophysics. **479**, 52–65 (2009). https://doi.org/10.1016/j.tecto.2009.01.026
6. R. Harris, J. Major, Waves of destruction in the East Indies: The Wichmann catalogue of earthquakes and tsunami in the Indonesian region from 1538 to 1877. Geol. Soc. Spec. Publ. **441**, 9–46 (2017). https://doi.org/10.1144/SP441.2
7. Badan Pusat Statistik Indonesia, Kecamatan Komodo dalam angka (BPS-Statistics of Manggarai Barat Regency, Manggarai Barat, 2024).
8. Pusat Gempa Nasional, Peta sumber dan bahaya gempa indonesia tahun 2017 (Pusat Penelitian dan Pengembangan Perumahan dan Permukiman, Bandung, 2017)
9. R.G. Harahap, Rekonstruksi dan simulasi penjalaran tsunami Banyuwangi 1994 menggunakan Mike 21 Flow Model. Inovtek Polbeng. **9,** 66 (2019). https://doi.org/10.35314/ip.v9i1.900
10. Badan Informasi Geospasial. Digital Elevation Model (DEM) dan Batimetri Nasional Retrieved on 2025 from tanahair.indonesia.go.id/portal-web/unduh/batnas
11. Danish Hydraulic Institute, MIKE 21 Toolbox. (2019).
12. B.C Papazachos, E.M. Scordilis, D.G. Panagiotopoulos, C.B. Papazacho, G.F. Karakaisis, Global relations between seismic fault parameters and moment magnitude of earthquakes, in Proceedings of the 10th International Congress Thessaloniki, April 2004, Bulletin of the Geological Society of Greece vol. XXXVI, Thessaloniki, Greece, April 15-17 (2004).
13. P.K. Boswood, Tsunami modelling along the East Queensland Coast. Coasts Ports 2013. 109–115 (2013).
14. T. Tursina, S. Syamsidik, S. Kato, M. Afifuddin, Influence of tides level on tsunami hydrodynamic in Banda Aceh, Indonesia, Int. J. Disaster Manag. **6**, 313–326 (2024). https://doi.org/10.24815/ijdm.v6i2.34538
15. X. Gao, X. Niu, Influence of tidal level on quantifying the probability of nearshore tsunami hazard. Ocean Eng. **266**, 3 (2022). https://doi.org/10.1016/j.oceaneng.2022.112986
16. W. Kongko, South Java Tsunami model using highly resolved data and probable tsunamigenic sources, Ph.D. thesis, Gottfried Wilhelm Leibniz University of Hannover, Faculty of Civil Engineering and Geodetic Science (2011)
17. S.J. Gibbons, S. Lorito, M. Asunción, M. Volpe, J. Selva, J. Macías, C. Sánchez-Linares, B. Brizuela, M. Vöge, R. Tonini, P. Lanucara, S. Glimsdal, F. Romano, J.C. Meyer, F. Løvholt. The Sensitivity of tsunami impact to earthquake source parameters and manning friction in high-resolution inundation simulations. **9**, 1–23 (2022). https://doi.org/10.3389/feart.2021.757618

18. L. Rasmussen, P.D. Bromirski, A.J. Miller, D. Arcas, R.E. Flick, M.C. Hendershott, Source location impact on relative tsunami strength along the U.S. West Coast,. J. Geophys. Res. Ocean. **120**, 4945–4961 (2015). https://doi.org/10.1002/2015JC010718
19. K. Zygmunt, Energy flux as a tool in locating tsunami secondary sources. Sci. Tsunami Hazards. **27**, 3, 1–29 (2008).
20. M. Lavrentiev, K. Lysakov, A. Marchuk, K. Oblaukhov, M. Shadrin. Dependence of tsunami wave maximal heights along a coastline on the source orientation. J. Phys. Conf. Ser. **1268** (2019). https://doi.org/10.1088/1742-6596/1268/1/012041
21. K.J. Horsburgh, C. Wilson, B.J. Baptie, A. Cooper, D. Cresswell, R.M.W. Musson, L. Ottemo¨ller, S. Richardson, S.L. Sargeant, Impact of a Lisbon-type tsunami on the U.K. coastline and the implications for tsunami propagation over broad continental shelves. J. Geophys. Res. Ocean. **113**, C04007 (2008). https://10.1029/2007JC004425